ENGINEERING

Direct gold bonding for flexible integrated electronics

Masahito Takakuwa[1,2], Kenjiro Fukuda[2,3]*, Tomoyuki Yokota[4], Daishi Inoue[2], Daisuke Hashizume[2], Shinjiro Umezu[1]*, Takao Someya[2,3,4]*

Flexible and stable interconnections are critical for the next generation of shape-conformable and wearable electronics. These interconnections should have metal-like conductivity and sufficiently low stiffness that does not compromise the flexibility of the device; moreover, they must be achieved using low-temperature processes to prevent device damage. However, conventional interconnection bonding methods require additional adhesive layers, making it challenging to achieve these characteristics simultaneously. Here, we develop and characterize water vapor plasma–assisted bonding (WVPAB) that enables direct bonding of gold electrodes deposited on ultrathin polymer films. WVPAB bonds rough gold electrodes at room temperature and atmospheric pressure in ambient air. Hydroxyl groups generated by the plasma assist bonding between two gold surfaces, allowing the formation of a strong and stable interface. The applicability of WVPAB-mediated connections to ultrathin electronic systems was also demonstrated, and ultraflexible organic photovoltaics and light-emitting diodes fabricated on separate films were successfully interconnected via ultrathin wiring films.

INTRODUCTION

The development of flexibility and stable interconnection technologies is becoming very important in flexible electronics with the evolution of high performance and thinness of individual devices (*1*–*3*). The electrical and mechanical properties of flexible sensors and power sources have improved markedly, and their performance is rapidly approaching that of rigid devices. Total device thicknesses are decreasing to the order of a few micrometers or less, making devices ultralightweight, soft, shape conformable, and nearly imperceptible when integrated into wearable electronics (*4*, *5*). Effective strategies for system-level integration are necessary to apply these devices to the next generation of on-skin electronics (*3*, *6*, *7*) and electronic textiles (*8*–*10*). In flexible electronics that are thin and have a large area, interconnecting each device fabricated on different films is more practical than sequentially fabricating the devices on one common substrate (*11*). Metal-like high conductivity, sufficient thinness without compromising the flexibility of the device, and low stiffness are the key requirements for such interconnections.

Conductive bonding technologies for electrodes on different flexible substrates include soldering, bonding via adhesive surrounded by conductive bumps (*12*, *13*), and the use of conductive solutions or composites of conductive filler mixed with adhesive (*12*, *14*, *15*). In these methods, heating and pressurization processes are usually required to cure the adhesive (or liquefy it in the case of solder) and achieve highly conductive bonds.

Direct metal bonding without any adhesive can be achieved with cold welding or surface-activated bonding (SAB). A large normal or frictional load and a pristine clean flat ductile surface in an ultrahigh vacuum environment are generally required to realize cold welding in bulk metals (*16*, *17*). SAB of metals typically requires very smooth surfaces [typical root mean square (RMS) roughness of <1 nm] and was developed primarily for flat sputtered metals on Si wafers (*18*–*23*). In both methods, metal oxides and metal hydroxides have no free electrons. Therefore, this bonding occurs only when the surface is pure metal. In addition, SAB could also be used for direct polymer bonding such as polydimethylsiloxane (PDMS). The functional groups on the surface are radicalized by plasma treatment. Additional covalent bonds are formed when the reactive radical species on the polymer and the metal surface contact each other (*24*, *25*).

However, direct metal-to-metal bonding on flexible substrates is hindered by many fundamental issues. The flatness of the metal on the polymeric flexible substrate usually has a roughness of several nanometers or more, which is not sufficiently flat for SAB. It is also difficult to achieve surfaces sufficiently clean for SAB of metals on polymer substrates as they have many contaminants from the polymers and the devices fabricated on the flexible substrate that are difficult to remove. Normal plasma treatment does not produce radicals on metal surfaces; hence, covalent bonding with reactive functional groups is not possible. Conversely, bonding with adhesives typically requires temperatures of 200°C, which limits the applicable polymer materials. Flexibility is also compromised owing to the stress concentration caused by the thickness and stiffness of the cured material.

Here, we present a method for achieving direct bonding of gold electrodes deposited on ultraflexible substrates. This bonding process is completed at room temperature and with no additional pressure; hence, there are no restrictions on the polymer material that can be used. Furthermore, high flexibility and high resolution of the bonded area are simultaneously achieved because there are no additional layers. The bond can withstand at least 10^4 bending cycles; it has excellent damp heat stability for more than 500 hours, confirming the compatibility of the process to a wide range of flexible electronic applications. To demonstrate the feasibility of this bonding technology, high-performance integrated systems of ultrathin organic light-emitting diodes (OLEDs) and organic photovoltaic (OPV) modules fabricated on separate flexible substrates were connected, showing no degraded performance.

[1]Department of Modern Mechanical Engineering, Waseda University, 3-4-1 Okubo, Shinjuku-ku, Tokyo 169-8555, Japan. [2]Center for Emergent Matter Science, RIKEN, 2-1 Hirosawa, Wako, Saitama 351-0198, Japan. [3]Thin-Film Device Laboratory, RIKEN, 2-1 Hirosawa, Wako, Saitama 351-0198, Japan. [4]Electrical and Electronic Engineering and Information Systems, The University of Tokyo, 7-3-1 Hongo, Bunkyo-ku, Tokyo 113-8656, Japan.
*Corresponding author. Email: kenjiro.fukuda@riken.jp (K.F.); umeshin@waseda.jp (S.U.); takao.someya@riken.jp (T.S.)

RESULTS

Water vapor plasma–assisted bonding of gold

A schematic of the direct gold bonding technology is shown in Fig. 1. We refer to this technology as a water vapor plasma–assisted bonding (WVPAB). The sample consisted of an evaporated Au electrode deposited on a 2-μm-thick parylene substrate. The surfaces of the two parylene films with Au electrode were treated with water vapor plasma (Fig. 1A) before being placed in contact with each other under ambient air (Fig. 1B). The gold-gold direct bonding was achieved by leaving it for approximately 12 hours or longer without additional heating and pressure. In contrast to the Au bonding, the overlapped parylene films were not bonded by WVPAB.

WVPAB achieved direct Au bonding with rough Au interface on ultrathin films. Surface morphology measurements with atomic force microscopy show that the RMS roughness of Au deposited on ultrathin parylene film was 6.3 nm (Fig. 2A). Figure 2B shows cross-sectional scanning electron microscopy (SEM) images of the areas bonded using WVPAB. Although a few voids were observed at the bonding interface, most of the interface was no longer visible. This indicated strong bonding between the two Au layers. Conversely, conventional SAB could not achieve bonding, leaving the films separated by a distinct interface (Fig. 2C). With smooth Au surfaces (RMS of 1.8 nm), WVPAB achieves perfect bonding without voids, whereas many voids were observed at the interface with conventional SAB (fig. S1). The void rate per 10 μm for each interface was estimated from cross-sectional SEM images (table S1 and fig. S2). The void rate is much lower than that of conventional SAB; thereby, the water vapor plasma bonding achieves superior bonding strength. In addition, oxygen plasma–treated Au surface (RMS of ~7 nm) could not achieve direct gold bonding (table S2). Ar plasma primarily causes physical etching, whereas oxygen and water vapor plasma induce chemical activation and physical etching. Whereas oxygen plasma oxidizes the gold surface (*20*), water vapor plasma can activate it through chemical reactions while preventing oxidation. Sheet resistance of the Cr did not increase after water vapor plasma treatment (table S3); this confirms that the oxidation of the Cr surface did not occur after the water vapor plasma treatment.

Analysis of Au—Au direct bonding

Gold surfaces before and after water vapor plasma treatment were analyzed by x-ray photoelectron spectroscopy (XPS) (Fig. 2D and fig. S3). There was no shift in the binding energy of Au 4f and C 1s after plasma treatment; the states of Au and C were not changed by water vapor plasma treatment (fig. S3, B and C). Conversely, the O 1s peak shifted from 530.7 eV before treatment to a higher binding energy of 531.9 eV after treatment (Fig. 2D). Elemental analysis confirmed that the ratio of C decreased slightly and the ratio of O increased slightly after water vapor plasma treatment (table S4). Furthermore, by curve fitting of the O 1s XPS signal, the binding states of O 1s before and after treatment were confirmed (Fig. 2D). As a result of analyzing the O 1s XPS signal of the plasma-treated sample using the untreated O 1s XPS signal as a component, an increase in binding energy peak at 531.9 eV assigned to O—H bonding was observed (*26*). Curve fitting of the treated gold surface revealed the generation of 23.7% O 1s groups and 76.3% O—H groups (Fig. 2D and table S5).

The bonding interface was also characterized using a high-resolution cross-sectional scanning transmission electron microscope (STEM). Two different regions along the interface of the bonded gold electrodes were identified: a region with a sharp color transition (region 1) (Fig. 2E) and a region with a smooth color transition (region 2) (Fig. 2E). The oxygen concentration in each region was determined using energy-dispersive x-ray spectroscopy. The oxygen concentration of region 1 was 1.0% higher than that of

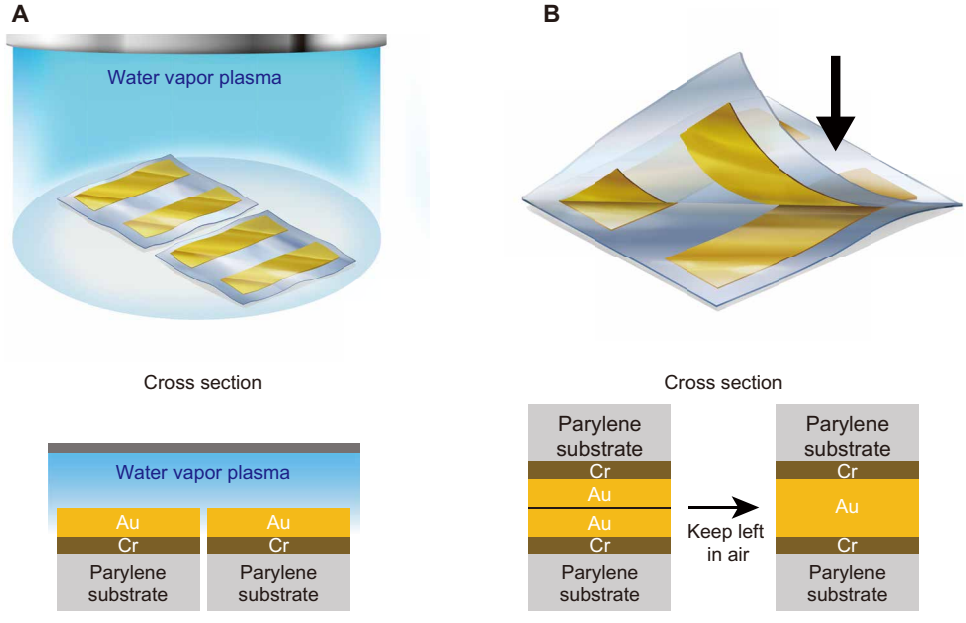

Fig. 1. Schematic illustration of direct Au bonding on flexible substrates using WVPAB. (**A**) Evaporated Au surfaces on 2-μm-thick parylene substrates were exposed to water vapor plasma. (**B**) Bonding of water vapor plasma–treated Au was achieved by overlapping the two substrates and storing them in ambient air for a few seconds to several hours without any applied pressure or heat.

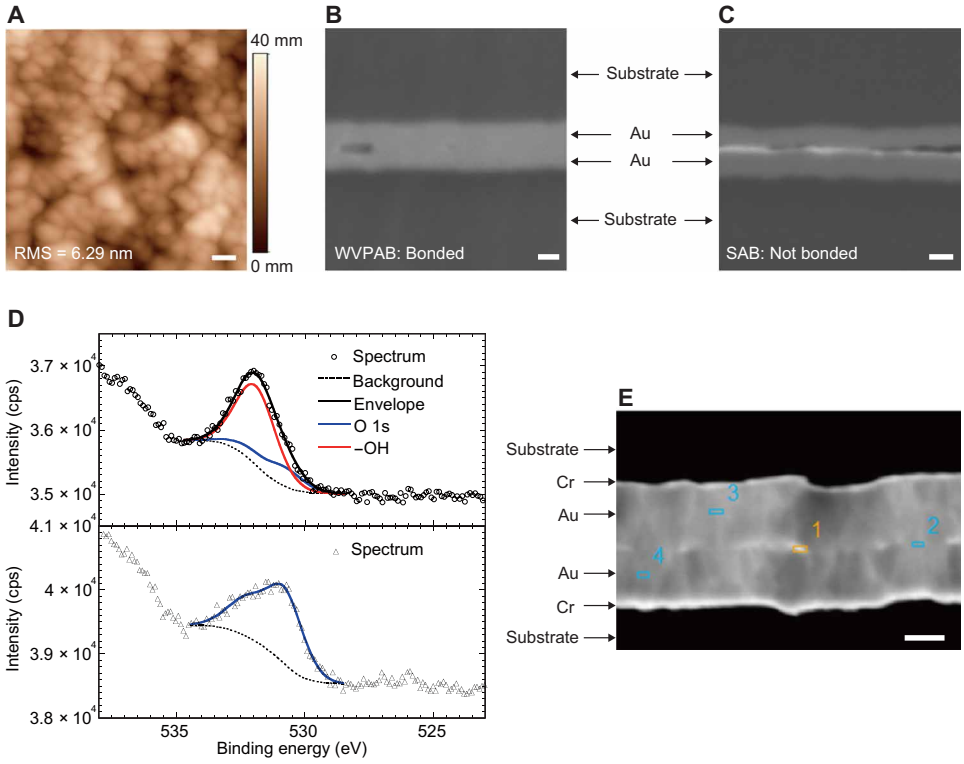

Fig. 2. Analysis of an Au—Au direct bonding by WVPAB. Au layers (100 nm thick) with two different surface roughness values were prepared. (**A**) Atomic force microscopy images of the rough (RMS of 6.29 nm) Au surfaces. (**B** and **C**) Cross-sectional SEM images of the interface of the two gold layers. (B) Interface of the rough Au films treated with WVPAB. (C) Interface of the rough Au films treated with conventional Ar SAB. (**D**) XPS analysis of O 1s on the gold surface. The top graph shows the XPS measurement result for a gold surface with water vapor plasma treatment; the bottom graph shows the XPS measurement result for a gold surface with no plasma treatment. cps, count per sec. (**E**) High-resolution cross-sectional image using STEM of the interface of the rough Au films bonded using WVPAB. There were two different regions along the interface: a region with a sharp color transition at the interface (region 1) and a region with a smooth color transition at the interface (region 2). Regions 3 and 4 show gold layer regions away from the interface. Scale bars, 100 nm.

region 2, as well as that of the other inner regions away from the interface (regions 3 and 4) (table S6).

Characterization of direct bonding by WVPAB

The effects of exposure time and atmosphere after water vapor plasma treatment were investigated. When the activated surface was stored in air, the activity decreased with time owing to the influence of deposits such as oxygen. In conventional SAB, the surfaces must be overlapped immediately after surface activation using Ar plasma (*27*). After water vapor plasma treatment, the samples were kept under one of three conditions: in ambient air, in a vacuum pack, and in a vacuum chamber. After storage, the films were overlapped for bonding. The maximum peeling strength of the bonded samples was evaluated by a 180° peeling test (fig. S4). Three failure modes, which depended on the atmosphere and exposure time, were observed. In the first mode, adhesive failure occurred when the metallic contacts were delaminated because they were insufficiently bonded (fig. S4A). In the second mode, substrate failure, the Au bond exhibited no adhesive failure; however, the supporting polymer film itself was torn (fig. S4C). This failure mode indicated that the bonding strength was higher than that of the ultrathin film used in this study. In the third mode, partial adhesive failure, the specimen had both bonded and unbonded areas: partially peeling off in some regions and tearing in others (fig. S4B). The relationship between the maximum peeling strength and storage time is shown in fig. S4D. The sample stored in the vacuum chamber exhibited no adhesive failure even after being stored for 100 hours before attachment, indicating good Au—Au bonding. The sample that was left in air for 1 hour before attachment exhibited adhesive failure. In contrast, the samples placed in ambient air using a vacuum pack exhibited almost no adhesive failure for up to 5 hours. A few of these samples exhibited mixed-mode failure after 40 hours. Therefore, storing the activated samples in high vacuum is an effective means of maintaining the activated state of the bonding surface and extending the acceptable time for achieving Au—Au direct bonding.

Electrical characteristic, mechanical durability, and thermal stability of WVPAB

To estimate the contact resistance of WVPAB, we prepared a bonded thin-film sample and a glass sample with Au wiring having the same thickness and pattern as the bonded sample (fig. S5). The wiring resistance was evaluated using a four-terminal measurement. The average wiring resistance of the bonded sample and reference gold wiring was 3.27 and 3.34 ohms, respectively (fig. S6). As both samples have similar total resistances, the contact resistance of WVPAB is negligibly small. In addition, the minimum feature sizes for electrical bonding were determined. The conductivity was evaluated by varying the length, *X*, of the overlapping area of the

two thin-film bonding specimens (fig. S7). The minimum conductive area of WVPAB is less than 50 μm by 50 μm (Fig. 3A), which is more than 100 times smaller than the feature size obtained using the conventional anisotropic conductive film (ACF) tape technique. Furthermore, the minimum line and space (*L*/*S*) evaluation revealed that 10 μm of *L*/*S* can be achieved using WVPAB (Fig. 3B and fig. S8). A linear current change as a function of voltage can be observed in two adhered electrodes, denoted as A and B in Fig. 3B, indicating good electrical bonding in narrow electrodes (Fig. 3C). Furthermore, complete insulation was demonstrated between adjacent electrodes, denoted as A and D in Fig. 3B, even at a short distance of 10 μm. These results show that WVPAB is capable of achieving higher-resolution bonding than those achieved using conventional methods.

To evaluate the thermal stability of WVPAB-induced conductive bonds, a high-temperature and high-humidity test [85°C, 85% relative humidity (RH)] was conducted. The electrical contact improved after storage under damp heat conditions for 505 hours, with resistance decreasing by as much as 7% (Fig. 3D). Similarly, after heating at 100°C in air for 555 hours, the electrical resistance decreased by 8% (Fig. 3E). These results show the excellent long-term stability of WVPAB-induced Au bonds even under harsh temperature and humidity conditions. The cross-sectional STEM images of the WVPAB-bonded substrate before and after heating at 100°C for 3 hours in air are shown in fig. S9. At the interface of Au/Au, oxygen-rich interface regions decreased, and areas with a smooth color transition became more prominent. Moreover, the independent gold grains before heating were changed to one large grain because of heating. Therefore, the contact resistance decreased, and the conductivity was enhanced by heating (Fig. 2E). In addition, as the gold grains were combined, the interface disappeared. Hence, it is considered that the bonding strength does not decline for a long period after bonding.

The mechanical robustness and flexibility of the bonded electrodes were also evaluated. Repeated bending cycles were applied to

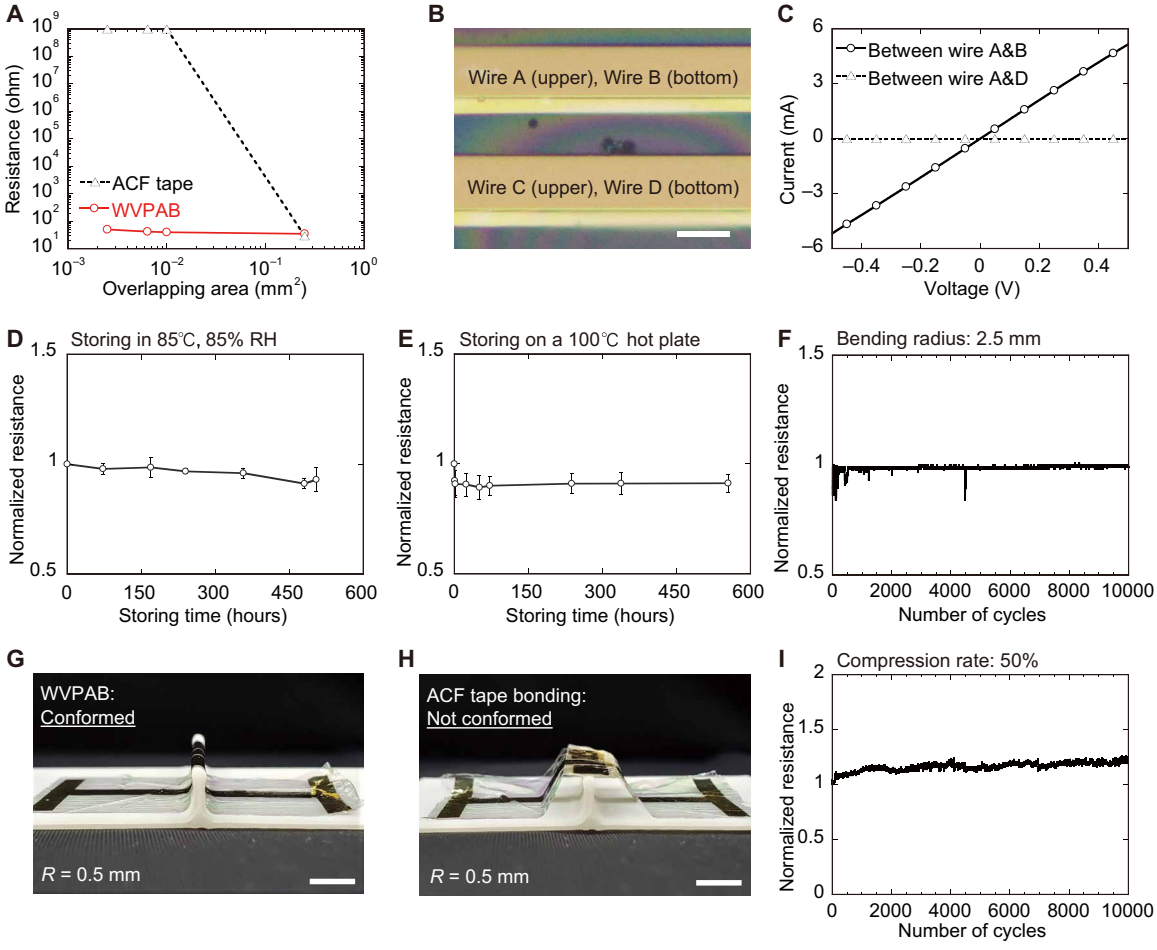

Fig. 3. Electrical and mechanical performance of the Au electrodes bonded using WVPAB. (**A**) Resistance as a function of the overlapping area. The black triangles represent the results obtained when the ACF tape was used, and the red circles represent the results obtained when WVPAB was used. (**B**) Top-view microscope image of the bonded electrodes with *L*/*S* of 10 μm. Scale bar, 10 μm. (**C**) Current-voltage (*I*-*V*) characteristics of the bonded electrodes shown in (B). Circles represent the *I*-*V* characteristics between wires A and B, and triangles represent the *I*-*V* characteristics between wires A and D. (**D**) Normalized resistance of the bonded electrodes as a function of storage time in 85°C and 85% RH. (**E**) Normalized resistance of the bonded electrodes as a function of heating time at 100°C. (**F**) Change in the normalized resistance after the cyclic bending test. The bonded region was bent with a bending radius of 2.5 mm. (**G** and **H**) Optical images of the conformability test on the curved surface (radius: 0.5 mm) of the thin films bonded using WVPAB (G) and using the ACF tape (H). Scale bars, 5 mm. (**I**) Changes in the normalized resistance in the electrode bonded using WVPAB during repeated 50% compression and release cycles. Photo credit: Masahito Takakuwa, Waseda University.

the bonded electrodes (fig. S10 and movie S1). The change in electrical resistance of the circuit was less than 1% after 10,000 bending cycles with a 2.5-mm bending radius (Fig. 3F). To evaluate the conformability of the curved surface with a small bending radius, films bonded using both WVPAB and ACF tape methods were adhered onto three-dimensional printed convex shapes (figs. S11 and S12, A and B). The films bonded using WVPAB showed perfect conformation even at a radius of 0.5 mm (Fig. 3G and fig. S12C), whereas those bonded using the ACF tape were not conformed for a radius less than or equal to 1 mm (Fig. 3H and fig. S12D).

Owing to this flexibility, ultrathin films could be applied to stretchable electronics using a buckling strategy. We attached the bonded electrodes to a prestretched elastomer and performed cyclic compression and release tests (*28*). After applying 50% compression/release for 10,000 cycles (fig. S13 and movie S2), the electrical resistance increased by 23% (Fig. 3I). These results confirm that the bonded electrodes achieve excellent mechanical flexibility, softness, and durability for stretchable electronics.

Fabrication of ultraflexible electronics system via the WVPAB method

We demonstrated the applicability of WVPAB-mediated connections to real-world ultrathin electronic systems (Fig. 4A). An ultrathin OPV module (fig. S14 and table S7) and an OLED (fig. S15) were fabricated on separate films and connected using five ultrathin wiring films (Fig. 4A and fig. S16A). WVPAB minimized the thickness of the entire device; therefore, components having large areas could be easily integrated into functional devices while maintaining excellent flexibility throughout the system (Fig. 4B and fig. S16B). Furthermore, the system operated successfully even after extreme mechanical strain was applied to the wiring films (movie S3). We quantitatively investigated the degradation of electronic devices after WVPAB by measuring the performance of the ultrathin OPV before and after water vapor plasma treatment (Fig. 4C). The ultraflexible OPV exhibited an initial power conversion efficiency of 10.6%, with a negligible change even after the water vapor plasma treatment (table S7). This shows that WVPAB technology can be used for fully integrated ultrathin electronics. In addition to connecting ultrathin devices, WVPAB methods could also be used as a mounting technology for attaching chip electronics to a flexible substrate. A chip LED was mounted on a patterned Au electrode that had been deposited on a 2-μm-thick parylene substrate. The LED lit up when voltage was applied, indicating effective interfacing between the prepackaged LED and the Au electrode (fig. S17 and movie S4).

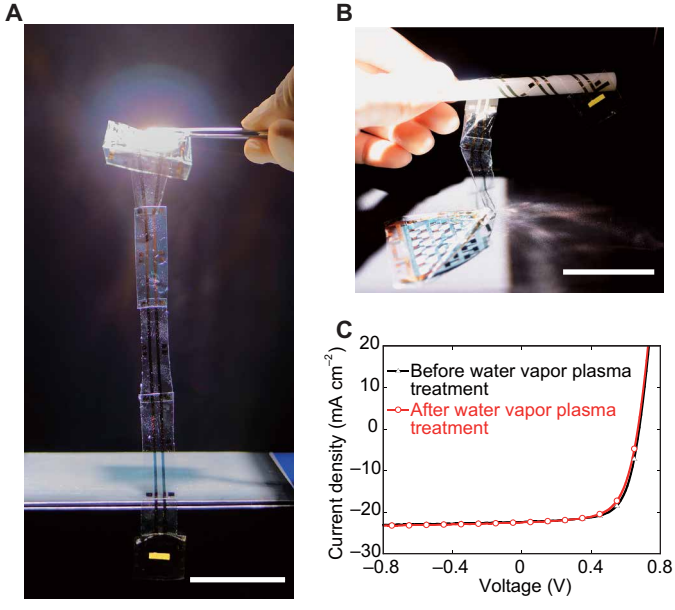

Fig. 4. Operation of an integrated device composed of two ultrathin electronic devices interconnected by WVPAB using ultrathin wiring films. (**A**) Optical image of the ultraflexible integrated system. An OPV, an OLED, and five wiring films were fabricated on different ultrathin substrates and then integrated using WVPAB. (**B**) Photograph of the integrated system being wrapped around a stick (radius of 10 mm). (**C**) Current density–voltage (*J-V*) characteristics of a single OPV cell before (black triangles) and after (red circles) the water vapor plasma treatment. Scale bars, 5 cm. Photo credit: Masahito Takakuwa, Waseda University.

DISCUSSION

We presented a flexible, high-resolution, and durable bonding technique for the integration of flexible or flexible-rigid hybrid systems. The Au surface evaporated on polymer substrates contained impurities, as observed in the XPS results. This can be attributed to the use of organic materials as substrates and high vacuum (in the range from 10^{-4} to 10^{-3} Pa) for the gold evaporation. As shown in Fig. 2C, conventional SAB could not achieve direct bonding of such Au surfaces. However, WVPAB could achieve direct gold bonding on these substrates. On the basis of the XPS results, the chemical bonding state of C 1s did not change before and after the plasma treatment (table S5 and fig. S3). Conversely, the ratio of oxygen atoms and the chemical bonding state of the hydroxyl groups increased with plasma treatment. Therefore, we consider that the hydroxyl group influences the direct bonding to the rough gold surface. Conversely, SAB only has a metallic bonding mechanism (*20*) requiring heavy contact; thereby, it could not be applied to rough interfaces.

The excellent flexibility of interconnections made by WVPAB comes from the thickness of the bonding area. The flexural rigidity or bending rigidity, D, is defined by the following equation (*29*)

$$D = \frac{Et^3}{12(1-\nu)} \quad (1)$$

where E, t, and ν denote the Young's modulus, thickness, and Poisson's ratio of the film, respectively (*29*). The increase in D arises from the increase in the thickness of the bonding area found in ACF-connected devices. D is proportional to the cube of the thickness of the film. The bonding area of the ACF tape can be bent by applying force; however, it will not bend under its weight like the bonding area of WVPAB. Thereby, the connection with ACF tapes does not have conformability. Hence, flexible electronics will not adhere well to complex curved surfaces such as the body or moving parts such as joints. This may lead to increased noise in the acquired biological signals and discomfort for the user. Therefore, it is essential for the entire system (electronics, wiring, and joints) to be flexible. The direct bonding of Au using WVPAB exhibited notably higher flexibility than all Electrically Conductive Adhesive (ECA)–mediated bonding methods, such as ACF tape bonding, by minimizing the thickness of

the system. The direct bonding of Au electrodes on 2-μm-thick films could be achieved with WVPAB.

This technique simplifies the integration of multiple flexible electronic devices on a single substrate and improves the flexibility of flexible devices attached using thick adhesive connections. Our proposed method can also be used for attaching chip electronics to flexible substrates. Although our study focused only on gold and parylene, this technology has the potential to become a general-purpose integration technology for a wide range of materials by tuning the plasma conditions and surface roughness of the electrodes for bonding.

MATERIALS AND METHODS

Fabrication of an ultrathin polymer substrate with a patterned gold sample

A 2-μm-thick parylene film (diX-SR, Daisan Kasei Co.) was deposited using chemical vapor deposition (CVD) (PDS 2010, Kisco) on a glass slide coated with a fluorinated polymer layer (Novec 1700, 3M). To create a flat Au surface (fig. S1), an epoxy solution was prepared by mixing epoxy (SU-8 3005, MicroChem) with solvent (SU-8 Developer, MicroChem) at a weight ratio of 1:1 for 30 s using a vortex mixer. A 500-nm layer of this epoxy solution was then spin-coated (5000 rpm for 60 s) on a 2-μm-thick parylene layer. The film was then exposed to ultraviolet (UV) light for 3 min and annealed at 95°C for another 3 min. Patterned Cr/Au electrodes were deposited on plain parylene and epoxy/parylene substrates using a thermal evaporator at a pressure below 1×10^{-3} Pa. A thin Cr layer was added to improve the adhesion strength of gold to the substrate (*30*). The thicknesses of Cr and Au are provided in the Supplementary Materials and Materials and Methods. Unless otherwise mentioned in the text, all results were obtained using thin-film samples of Cr/Au with large surface roughness values (Fig. 2A) deposited on plain parylene substrates.

WVPAB procedure

The ultrathin polymer substrate with patterned gold samples was delaminated using a knife and a tweezer from the glass plate. The surfaces of the two parylene films with electrode were treated with water vapor plasma (Aqua Plasma Cleaner AQ-500, Samco Inc.) under the following conditions: 50 W of plasma power, 12 sccm (standard cubic centimeters per minute) of gas flow, 40 s of plasma treatment time, and 10 Pa of pressure. After water vapor plasma treatment, samples were taken out from the machine into ambient air, and the gold surfaces were subsequently overlapped. To contact the two gold surfaces uniformly, the overlapped area was pressed using a finger (ca. 2 N of force for 5 s). Subsequently, the gold-gold direct bonding was achieved by leaving it for 12 hours or longer without additional heating and pressing. For all experiments, the films were stored in ambient air for 12 to 48 hours after the evaporation of gold before the water vapor plasma process. The adhesion results were independent of the storage times within the aforementioned range.

Bonding alignment

In the case of the experiments related to resolution, we used a mask aligner for alignment. A PDMS elastomer (DOWSIL SILPOT 184 W/C) was prepared by mixing with a curing agent (DOWSIL SILPOT 184 W/C) in the ratio 10:1. The elastomer was degassed in a vacuum chamber for 10 min and spin-coated (3000 rpm, 60 s) onto the glass. The sample was annealed at 100°C for 1 hour. Part of the PDMS was removed from the glass (fig. S18) using a knife. Following the WVPAB procedure, we prepared plasma-treated samples. One of the samples was fixed onto the PDMS glass plate. The glass plate with a film sample was kept on the base plate for the mask in the mask aligner (ES410, Nanometric Technology Inc.). The other water plasma–treated film sample was fixed on the base plate for the sample. The base plate for fixing the mask was moved, and the alignment was carried out using the *X*, *Y*, and θ knobs of the microscope. After alignment, the two film samples were slowly contacted and bonded using the *Z* handle. The two film samples were precisely overlapped. In the case of other experiments, we conducted the alignment manually using tweezers under a microscope.

Comparison of gas sources of plasmas for bonding of gold with rough surfaces

We prepared the thin-film samples with thin chrome (3.5 nm), and gold (100 nm) was evaporated onto the 2-μm-thick parylene substrate. The plasma conditions for oxygen and argon plasma were similar to those used for the WVPAB process. Each bonding procedure follows the WVPAB process. The bonding of the samples was confirmed by peeling tests using tweezers after the bonding was completed.

SEM and STEM measurement

A specimen for the cross-sectional observation of the bonded sample was prepared using an ion beam milling system (EM TIC 3X, Leica) and a microtome (Ultracut UCT, Leica). The SEM images were obtained using the ultraversatile high-resolution SEM (Quattro S, Thermo Fisher Scientific) with an acceleration voltage of 2 kV. The STEM images were obtained with an acceleration voltage of 30 kV.

XPS analysis

Plasma-treated and untreated ultrathin gold on polymer films for storing in a vacuum pack was prepared. XPS measurement [KRATOS ULTRA 2 (AXIS Supra), Shimadzu Co.] was started 5 hours after vacuum packing.

Storing condition for evaluating the influence of exposure time and atmosphere

After water vapor plasma treatment, the samples were kept under one of three conditions: in ambient air, a vacuum pack, and a vacuum chamber. In the case of ambient air, samples were kept in ambient air after plasma treatment. In the case of vacuum pack, samples were taken out from the chamber into the air after plasma treatment and were immediately packed into an aluminum bag with a vacuum packing machine (FCB-200, Fuji Impulse Co. Ltd.; vacuum degree: around 1000 Pa). The vacuum-packed aluminum bag in samples was then left in the atmosphere (fig. S19). After the predetermined time had elapsed, the samples were taken out; the plasma-treated surfaces were immediately bonded in ambient air. In the case of the vacuum chamber, treated samples remained in the chamber of water vapor plasma after the plasma process under vacuum (10 Pa). They were not exposed to the atmosphere after plasma treatment. After the predetermined time had elapsed, the chamber was vented and the samples were taken out. The plasma-treated surfaces were then immediately contact-bonded in ambient air.

180° peeling test

A 7 mm–by–12 mm layer of Cr (3.5 nm)/Au (50 nm) was evaporated onto a 2-μm-thick parylene substrate. After bonding the electrodes together using WVPAB under each condition, the maximum peeling strength was measured using a tensile shear test (EZ-LX, Shimadzu Co.). The peeling speed was 10 mm/min.

Cyclic bending test

A bonded thin-film sample was prepared using WVPAB (fig. S10, A and B). The sample was placed on a 50-μm-thick supporting film to apply a constant bending radius (2.5 mm), which was subsequently fixed to a moveable stage (fig. S10C). The sample was also connected to a constant-current circuit with a three-terminal regulator as a resistor in series. The voltage across the sample was measured for each 1-mm movement of the movable stage, and the electrical resistance of the sample was calculated using the voltage. The movable stage was moved 10 mm in one direction at 20 mm/s.

Cyclic compression and release test

A bonded thin-film sample, similar to that used in the cyclic bending test, was prepared. Part of the exposed gold wiring was covered with additional parylene using CVD to prevent damage because of compression. Both ends of the gold wiring were connected to the external wires using the ACF tape to evaluate the degradation of only the bonded area (fig. S13, A and B). The bonded sample was placed on a 200% prestretched elastomer (VHB, 3M) and fixed to the experimental machine as shown in fig. S13C. A 50% compression strain, directed orthogonal to the current flow, was applied to the samples. The bonded sample acting as a resistor was connected in series in a constant-current circuit using a three-terminal regulator. The voltage across the bonded sample was measured using an Arduino microcontroller for every 5-mm movement of the movable table. This voltage was used to calculate the electrical resistance.

Fabrication of an ultraflexible OPV module

A 1-μm-thick parylene film (diX-SR, Daisan Kasei Co.) was deposited by CVD on a glass plate with a surface coated in a fluorinated polymer layer (Novec 1700, 3M). A 500-nm-thick layer of an SU-8 solution was deposited as a planarization layer. For the bottom electrode, a 100-nm-thick layer of indium tin oxide (ITO) was sputtered without substrate heating and patterned using photolithography and a wet etching process. Cr/Au electrodes (3.5-nm-thick Cr and 100-nm-thick Au) were fabricated as contact pads on the ITO layer using a thermal evaporator at a pressure below 1×10^{-3} Pa. Subsequently, a 20-nm-thick ZnO layer was used as the electron-transporting layer. The substrates were coated with a ZnO precursor by spin-coating (5000 rpm for 30 s). A precursor solution was prepared by dissolving zinc acetate dehydrate (0.5 g) and ethanolamine (0.16 ml) in 5 ml of 2-methoxyethanol. The substrates were then baked in air at 180°C for 25 min. An active layer solution was prepared by dissolving poly[4,8-bis(5-(2-ethylhexyl) thiophen-2-yl) benzo[1,2-*b*;4,5-*b*′]dithiophene-2,6-diyl-alt-(4-octyl-3-fluorothieno[3,4-b] thiophene)-2-carboxylate-2-6-diyl] (PBDTTT-OFT) (10 mg) and 2,2′-((2*Z*,2′*Z*)-(((4,4,9,9-tetrakis(4-hexylphenyl)-4,9-dihydro-sindaceno[1,2-*b*:5,6-*b*′]dithiophene-2,7-diyl)bis(4-((2-ethylhexyl) oxy)thiophene-5,2-diyl)) bis(methanylylidene))bis(5,6-difluoro-3-oxo-2,3-dihydro-1*H*-indene-2,1-diylidene))dimalononitrile (IEICO-4F) (15 mg) in 970 μl of chlorobenzene and 30 μl of 1-chloronaphthalene for 1.5 hours at 70°C and 400 rpm and subsequently spin-coated in a glove box at 1400 rpm for 60 s. After spin-coating, the OPV device was dried for 0.5 hours in a dark vacuum chamber, which yielded a 100-nm-thick photoactive layer. MoO_X (7.5 nm) and Ag (100 nm) were sequentially deposited using thermal evaporation below 3×10^{-4} Pa to form a hole-transporting layer and an anode, respectively. A 1-μm-thick parylene layer was deposited using CVD to form a passivation layer. Last, an Au electrode (30-nm-thick Au) serving as the bonding pad was deposited onto the Au electrodes using a thermal evaporator at a pressure below 1×10^{-3} Pa.

Fabrication of an ultraflexible OLED

A 1-μm-thick parylene film (diX-SR, Daisan Kasei Co.) was deposited using CVD to form an ultrathin substrate glass plate with a surface coated in a fluorinated polymer layer (Novec 1700, 3M). An epoxy solution was prepared by mixing epoxy (SU-8 3005, MicroChem) with a solvent (SU-8 Developer, MicroChem) in a weight ratio of 1:1 for 30 s using a vortex mixer. A 500-nm-thick SU-8 layer was spin-coated (5000 rpm for 60 s) to form a planarization layer. After spin-coating, the SU-8 layer was prebaked at 95°C for 3 min followed by UV exposure and post-baking (95°C for another 3 min). A 100-nm-thick layer of the bottom ITO electrode was sputtered without substrate heating and patterned using photolithography and a wet etching process. Cr/Au electrodes (5-nm-thick Cr and 50-nm-thick Au) were fabricated as contact pads on the ITO layer using a thermal evaporator at a pressure below 1×10^{-3} Pa. Plexcore OC AQ-1200 (Sigma-Aldrich) was spin-coated (1200 rpm for 40 s) and then annealed at 170°C for 15 min in ambient air. Poly[(9,9-dioctylfluorenyl-2,7-diyl)-co-(4,4′-(*N*-(4-sec-butylphenyl)diphenylamine)] (TFB) was spin-coated (1500 rpm for 60 s) using an *o*-xylene solution (10 mg/ml) and then annealed at 180°C for 60 min in nitrogen, producing a 10- to 20-nm-thick electron-blocking layer. A 70-nm-thick layer of Super Yellow was deposited via spin-coating (2000 rpm for 60 s) using a toluene solution of 6 mg/ml as the emissive layer. Last, NaF (1 nm) and Al (100 nm) were deposited as cathodes.

Device characterization

The current density–voltage (*J-V*) characteristics of the OPVs were recorded under AM 1.5G (100 mW cm^{-2}; with the intensity calibrated using a silicon reference solar cell) using a Keithley 2400 source meter under ambient laboratory conditions. To evaluate the OLED characteristics, a light distribution measurement system (C9920-11, Hamamatsu Photonics) and an external quantum efficiency measurement system (C9920-12, Hamamatsu Photonics) were used.

An integrated system of ultrathin electronics connected using WVPAB

Cr (3.5 nm)/Au (30 nm) was evaporated onto 2-μm-thick parylene to serve as an ultraflexible wire that connected the ultraflexible OPV module and the ultraflexible OLED (fig. S15). There were five wires in the integrated system of ultrathin electronics, and each connection was bonded using WVPAB. A solar simulator was used to perform the OLED operation experiment, using the OPV module as a power source.

Evaluation of the water vapor plasma treatment–induced degradation of the OPVs

OPVs with active areas of 0.04 cm^2 were fabricated using the same method as that used for making the OPV module. The initial *J-V*

characteristics of the OPVs were recorded under AM 1.5G (100 mW cm^{-2}; with the intensity calibrated using a silicon reference solar cell) using a Keithley 2400 source meter under ambient laboratory conditions. The *J-V* characteristics of the OPVs after the water vapor plasma treatment were also similarly measured to evaluate the performance degradation caused by the water vapor plasma treatment (plasma conditions: 12 sccm, 50 W, 40 s, 10 Pa) (Fig. 4C and table S7).

SUPPLEMENTARY MATERIALS

Supplementary material for this article is available at https://science.org/doi/10.1126/sciadv.abl6228

REFERENCES AND NOTES

1. T. Yokota, K. Fukuda, T. Someya, Recent progress of flexible image sensors for biomedical applications. *Adv. Mater.* **33**, 2004416 (2021).
2. T. R. Ray, J. Choi, A. J. Bandodkar, S. Krishnan, P. Gutruf, L. Tian, R. Ghaffari, J. A. Rogers, Bio-integrated wearable systems: A comprehensive review. *Chem. Rev.* **119**, 5461–5533 (2019).
3. J. Y. Oh, Z. Bao, Second skin enabled by advanced electronics. *Adv. Sci.* **6**, 1900186 (2019).
4. D.-H. Kim, J. Viventi, J. J. Amsden, J. Xiao, L. Vigeland, Y.-S. Kim, J. A. Blanco, B. Panilaitis, E. S. Frechette, D. Contreras, D. L. Kaplan, F. G. Omenetto, Y. Huang, K.-C. Hwang, M. R. Zakin, B. Litt, J. A. Rogers, Dissolvable films of silk fibroin for ultrathin conformal bio-integrated electronics. *Nat. Mater.* **9**, 511–517 (2010).
5. M. Takakuwa, S. W. Heo, K. Fukuda, K. Tajima, S. Park, S. Umezu, T. Someya, Nanograting structured ultrathin substrate for ultraflexible organic photovoltaics. *Small Methods* **4**, 1900762 (2020).
6. S. Hong, H. Lee, J. Lee, J. Kwon, S. Han, Y. D. Suh, H. Cho, J. Shin, J. Yeo, S. H. Ko, Highly stretchable and transparent metal nanowire heater for wearable electronics applications. *Adv. Mater.* **27**, 4744–4751 (2015).
7. Y. Liu, M. Pharr, G. A. Salvatore, Lab-on-Skin: A review of flexible and stretchable electronics for wearable health monitoring. *ACS Nano* **11**, 9614–9635 (2017).
8. T.-G. La, S. Qiu, D. K. Scott, R. Bakhtiari, J. W. P. Kuziek, K. E. Mathewson, J. Rieger, H.-J. Chung, Two-layered and stretchable e-textile patches for wearable healthcare electronics. *Adv. Healthc. Mater.* **7**, 1801033 (2018).
9. N. Karim, S. Afroj, A. Malandraki, S. Butterworth, C. Beach, M. Rigout, K. S. Novoselov, A. J. Casson, S. G. Yeates, All inkjet-printed graphene-based conductive patterns for wearable e-textile applications. *J. Mater. Chem. C.* **5**, 11640–11648 (2017).
10. T. Koshi, K. Nomura, M. Yoshida, Electronic component mounting for durable e-textiles: Direct soldering of components onto textile-based deeply permeated conductive patterns. *Micromachines (Basel)* **11**, 209 (2020).
11. Y. Yamamoto, S. Harada, D. Yamamoto, W. Honda, T. Arie, S. Akita, K. Takei, Printed multifunctional flexible device with an integrated motion sensor for health care monitoring. *Sci. Adv.* **2**, e1601473 (2016).
12. S.-C. Kim, Y.-H. Kim, Review paper: Flip chip bonding with anisotropic conductive film (ACF) and nonconductive adhesive (NCA). *Curr. Appl. Phys.* **13**, S14–S25 (2013).
13. S.-M. Lee, B.-G. Kim, Y.-H. Kim, Non-conductive adhesive (NCA) trapping study in chip on glass joints fabricated using Sn bumps and NCA. *Mater. Trans.* **49**, 2100–2106 (2008).
14. J. S. Lee, S. J. Kang, J. H. Shin, Y. J. Shin, B. Lee, J.-M. Koo, T.-i. Kim, Nanoscale-dewetting-based direct interconnection of microelectronics for a deterministic assembly of transfer printing. *Adv. Mater.* **32**, 1908422 (2020).
15. K. M. Razeeb, J. Tao, F. Stam, Nanowire ACF for ultrafine-pitch flip-chip interconnection, in *Nanopackaging* (Springer International Publishing, 2018), pp. 701–723.
16. Y. Lu, J. Y. Huang, C. Wang, S. Sun, J. Lou, Cold welding of ultrathin gold nanowires. *Nat. Nanotechnol.* **5**, 218–224 (2010).
17. C. Kim, P. E. Burrows, S. R. Forrest, Micropatterning of organic electronic devices by cold-welding. *Science* **288**, 831–833 (2000).
18. T. Matsumae, Y. Kurashima, H. Takagi, Surface activated bonding of Ti/Au and Ti/Pt/Au films after vacuum annealing for MEMS packaging. *Microelectron. Eng.* **197**, 76–82 (2018).
19. E. Higurashi, K. Okumura, Y. Kunimune, T. Suga, K. Hagiwara, Room-temperature bonding of wafers with smooth Au thin films in ambient air using a surface-activated bonding method. *IEICE Trans. Electron.* **E100.C**, 156–160 (2017).
20. M. Yamamoto, T. Matsumae, Y. Kurashima, H. Takagi, T. Suga, T. Itoh, E. Higurashi, Comparison of argon and oxygen plasma treatments for ambient room-temperature wafer-scale Au–Au bonding using ultrathin Au films. *Micromachines (Basel)* **10**, 119 (2019).
21. M. Yamamoto, T. Matsumae, Y. Kurashima, H. Takagi, T. Suga, S. Takamatsu, T. Itoh, E. Higurashi, Effect of Au film thickness and surface roughness on room-temperature wafer bonding and wafer-scale vacuum sealing by Au-Au surface activated bonding. *Micromachines (Basel)* **11**, 454 (2020).
22. H. Takagi, R. Maeda, T. R. Chung, N. Hosoda, T. Suga, Effect of surface roughness on room-temperature wafer bonding by Ar beam surface activation. *Jpn. J. Appl. Phys.* **37**, 4197–4203 (1998).
23. A. Shigetou, T. Suga, Vapor-assisted surface activation method for homo- and heterogeneous bonding of Cu, SiO_2, and polyimide at 150°C and atmospheric pressure. *J. Electron. Mater.* **41**, 2274–2280 (2012).
24. L. Xiong, P. Chen, Q. Zhou, Adhesion promotion between PDMS and glass by oxygen plasma pre-treatment. *J. Adhes. Sci. Technol.* **28**, 1046–1054 (2014).
25. H. Terai, R. Funahashi, T. Hashimoto, M. Kakuta, Heterogeneous bonding between cyclo-olefin polymer (COP) and glass-like substrate by newly developed water vapor-assisted plasma, aqua plasma cleaner. *Electr. Eng. Japan.* **205**, 48–56 (2018).
26. G. Carraro, D. Barreca, A. Gasparotto, C. Maccato, Ag and Pt particles sputtered on β-Fe_2O_3: An XPS investigation. *Surf. Sci. Spectra* **19**, 1–12 (2012).
27. Y.-H. Wang, M. R. Howlader, K. Nishida, T. Kimura, T. Suga, Study on Sn–Ag oxidation and feasibility of room temperature bonding of Sn–Ag–Cu solder. *Mater. Trans.* **46**, 2431–2436 (2005).
28. M. Kaltenbrunner, T. Sekitani, J. Reeder, T. Yokota, K. Kuribara, T. Tokuhara, M. Drack, R. Schwödiauer, I. Graz, S. Bauer-Gogonea, S. Bauer, T. Someya, An ultra-lightweight design for imperceptible plastic electronics. *Nature* **499**, 458–463 (2013).
29. K. Fukuda, K. Yu, T. Someya, The future of flexible organic solar cells. *Adv. Energy Mater.* **10**, 2000765 (2020).
30. J. D. Yeager, D. J. Phillips, D. M. Rector, D. F. Bahr, Characterization of flexible ECoG electrode arrays for chronic recording in awake rats. *J. Neurosci. Methods* **173**, 279–285 (2008).

Acknowledgments: We thank Toray Industries Inc. for supplying the polymer (PBDTTT-OFT) used in our OPVs. We thank Shimadzu Co. for help with XPS measurements. We would like to thank M. Koizumi of the University of Tokyo (Japan), S. Watanabe of the Shimadzu Co. (Japan), and H. Terai of the Samco Inc. (Japan) for their technical support and aid in discussions. We would also like to thank S. I. Rich of RIKEN (Japan) for editing and proofreading the manuscript. **Funding:** This work was funded by Grants-in-Aid for Scientific Research (KAKENHI), grant JP18H05469, of the Japan Society for the Promotion of Science (JSPS); Adaptable and Seamless Technology Transfer Program through Target-driven R&D (A-STEP), grant A3015021R, of the Japan Science and Technology Agency (JST); Grant-in-Aid for JSPS Research Fellow Number JP21J21947; and Waseda Research Institute for Science and Engineering, Grant-in-Aid for Young Scientists (Early Bird). **Author contributions:** M.T., K.F., and T.S. designed the study. M.T., T.Y., D.I., and D.H. performed the experiments. M.T., K.F., and T.S. analyzed data. M.T., K.F., T.Y., S.U., and T.S. wrote the paper. **Competing interests:** M.T., K.F., and T.S. are coinventors on a patent application related to this work (Japanese patent application number 2021-6995, 20 January 2021). The authors declare no other competing interests. **Data and materials availability:** All data needed to evaluate the conclusions in the paper are present in the paper and/or the Supplementary Materials.

Submitted 26 July 2021
Accepted 5 November 2021
Published 22 December 2021
10.1126/sciadv.abl6228